THE ASTROPHYSICAL JOURNAL, 464:L5–L9, 1996 June 10

MICROWAVE EMISSION AT HIGH GALACTIC LATITUDES IN THE FOUR-YEAR DMR SKY MAPS

A. KOGUT,[1,2] A. J. BANDAY,[1,3] C. L. BENNETT,[4] K. M. GÓRSKI,[1,5] G. HINSHAW,[1] G. F. SMOOT,[6] AND E. L. WRIGHT[7]
Received 1996 January 11; accepted 1996 March 22

ABSTRACT

We use the *COBE*[8] Differential Microwave Radiometers (DMR) 4 yr sky maps to model Galactic microwave emission at high latitudes ($|b| > 20°$). Cross-correlation of the DMR maps with Galactic template maps detects fluctuations in the high-latitude microwave sky brightness with the angular variation of the DIRBE far-infrared dust maps and a frequency dependence consistent with a superposition of dust and free-free emission. We find no significant correlations between the DMR maps and various synchrotron templates. On the largest angular scales (e.g., quadrupole), Galactic emission is comparable in amplitude to the anisotropy in the cosmic microwave background (CMB). The CMB quadrupole amplitude, after correction for Galactic emission, has amplitude $Q_{\rm rms} = 10.7$ μK with random uncertainty 3.6 μK and systematic uncertainty 7.1 μK from uncertainty in our knowledge of Galactic microwave emission.

Subject headings: cosmic microwave background — cosmology: observations — Galaxy: general — ISM: general

1. INTRODUCTION

Diffuse microwave emission at high Galactic latitudes is dominated by the cosmic microwave background (CMB) and optically thin emission from Galactic synchrotron, dust, and free-free emission. These components may be distinguished by their different spatial morphology and frequency dependence. Synchrotron radiation dominates radio-frequency surveys, but the spectral index $\beta_{\rm synch}$ steepens with frequency and has poorly determined spatial variation (Banday & Wolfendale 1991; Bennett et al. 1992; Davies, Watson, & Gutiérrez 1996). Dust emission dominates far-infrared surveys, but its spectral behavior at longer wavelengths depends on the shape, composition, and size distribution of the dust grains, which are poorly known (Désert, Boulanger, & Puget 1990). Free-free emission from electron-ion interactions in the warm ionized interstellar medium (WIM) has well-determined spectral behavior but lacks a useful template map. At least one component of the WIM is spatially correlated with the far-infrared dust distribution on large angular scales (Kogut et al. 1996a); however, the fraction of the total WIM contained in the correlated component has substantial uncertainties. In this Letter we derive models of Galactic emission based on Galaxy-dominated sky surveys and the 4 yr *COBE* DMR microwave maps.

2. TECHNIQUES

We apply a cross-correlation technique to search the 4 yr DMR sky maps for emission whose spatial distribution is traced by a "template" map dominated by a single Galactic emission component. Unless otherwise stated, we use only the region $|b| > 20°$ with extended "custom" cutouts near Orion and Ophiuchus (Bennett et al. 1996). We use three templates (Fig. 1 [Pl. L4]): the synchrotron-dominated 408 MHz survey (Haslam et al. 1981), a "cosmic-ray" synchrotron model (Bennett et al. 1992) with spatially varying, frequency-dependent spectral index $\beta_{\rm synch}$, and the dust-dominated DIRBE 140 μm survey, from which a model of zodiacal dust emission has been removed (Reach et al. 1995). All templates are convolved with the DMR beam prior to analysis.

We assume that the DMR maps are a superposition of CMB emission and Galactic emission, $\Delta T^{\rm DMR} = \Delta T^{\rm CMB} + \alpha \Delta X^{\rm Gal}$, where $\Delta T^{\rm DMR}$ is the antenna temperature in a DMR map, $\Delta X^{\rm Gal}$ is the intensity of the Galactic template map (not necessarily in temperature units), and the coefficient α converts the units of the Galactic map to antenna temperature at the DMR frequency. Kogut et al. (1996a) estimate the correlation coefficient α by minimizing

$$\chi^2 = \sum_{a,b} (C - \alpha A)_a (\boldsymbol{M}^{-1})_{ab} (C - \alpha A)_b \,, \qquad (1)$$

where $C(\theta)$ is the cross-correlation function between the DMR map and Galactic template, $A(\theta)$ is the autocorrelation of the template map, $\boldsymbol{M}$ is the covariance matrix of the cross-correlation, and the indices a and b run over the angular bins of the correlation functions. In this Letter, we generalize equation (1) to use both a Fourier representation and the pixel temperatures of the high-latitude sky. That is, we minimize

$$\chi^2 = \sum_{a,b} (D - \alpha G)_a (\boldsymbol{M}^{-1})_{ab} (D - \alpha G)_b \,, \qquad (2)$$

where D is a linear function of the DMR map temperatures, G is a similar function for the Galactic template map, and $\boldsymbol{M}$ is the covariance matrix of the function D. The functions D and G are either the 961 Fourier components in an orthogonal basis (Górski et al. 1996) or simply the temperature in each

[1] Hughes STX Corporation, Laboratory for Astronomy and Solar Physics, Code 685, NASA/GSFC, Greenbelt, MD 20771.
[2] kogut@stars.gsfc.nasa.gov.
[3] Current address: Max-Planck-Institut für Astrophysik, Karl-Schwarzschild-Strasse 1, 85740 Garching bei München, Germany.
[4] Laboratory for Astronomy and Solar Physics, Code 685, NASA/GSFC, Greenbelt, MD 20771.
[5] On leave from Warsaw University Observatory, Aleje Ujazdowskie 4, 00-478 Warsaw, Poland.
[6] Department of Physics, Lawrence Berkeley Laboratory, Space Sciences Laboratory, and Center for Particle Astrophysics, Building 50-351, University of California, Berkeley, CA 94720.
[7] UCLA Department of Astronomy, P.O. Box 951562, Los Angeles, CA 90095-1562.
[8] The National Aeronautics and Space Administration/Goddard Space Flight Center (NASA/GSFC) is responsible for the design, development, and operation of the *Cosmic Background Explorer* (*COBE*). Scientific guidance is provided by the *COBE* Science Working Group. GSFC is also responsible for the analysis software and for the production of the mission data sets.

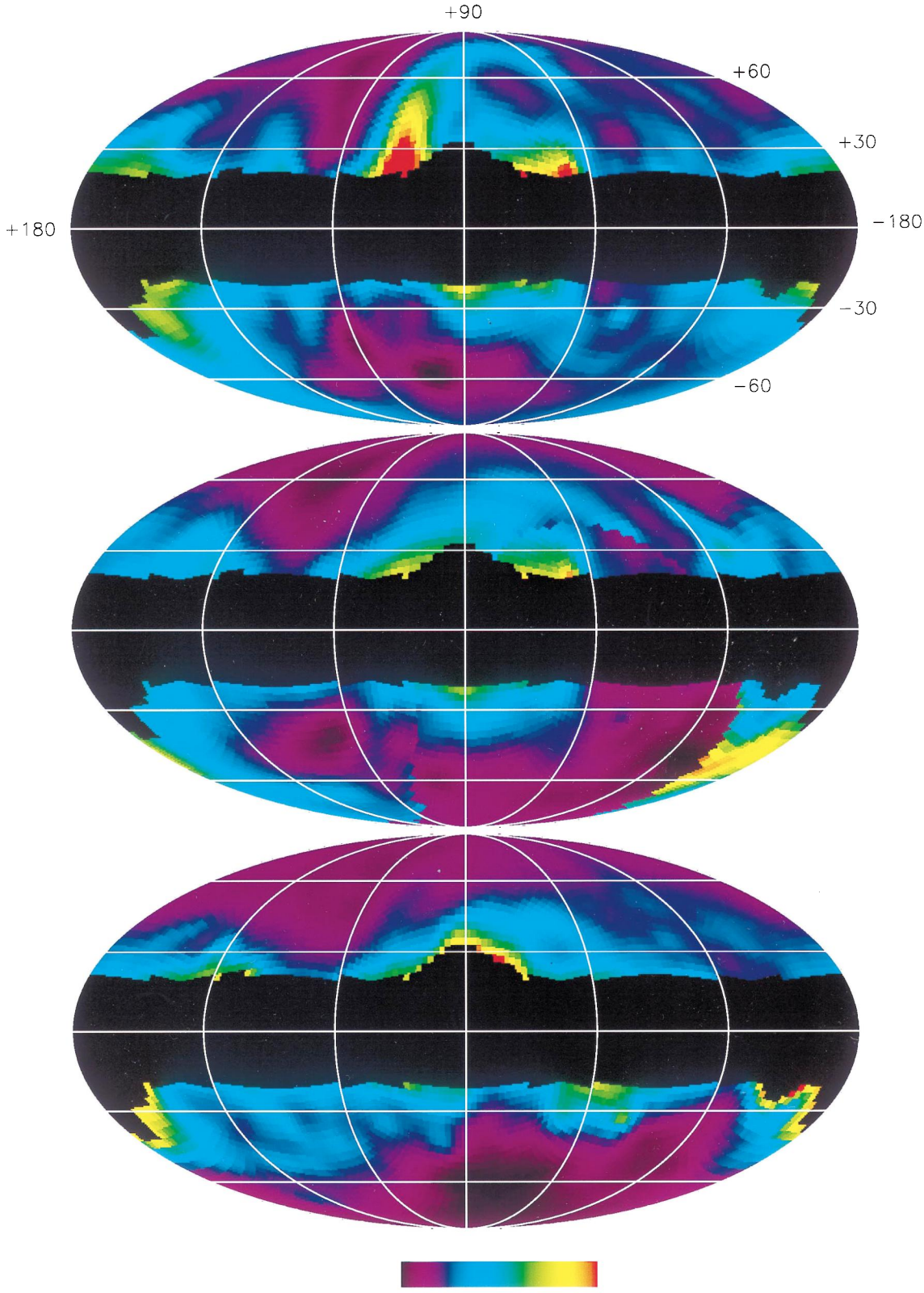

FIG. 1.—Galactic templates used in cross-correlation technique; Mollweide projection in Galactic coordinates. *Top*: Synchrotron-dominated 408 MHz survey. *Middle*: Cosmic-ray synchrotron model. *Bottom*: Dust-dominated DIRBE 140 μm survey. Each template has been convolved with the DMR beam pattern and is masked to show only data at high Galactic latitudes; a fitted monopole and dipole have been removed from the remaining pixels. The color transfer for each template runs 6 standard deviations from the coldest pixel.

KOGUT et al. (see 464, L5)

TABLE 1

DMR–Galactic Template Cross-Correlation Coefficients[a]

DMR Frequency (GHz)	Galactic Template		
	408 MHz[b]	Cosmic Ray[c]	DIRBE 140 μm[d]
31.5	1.17 ± 1.13	1.88 ± 1.24	6.37 ± 1.52
53	0.69 ± 0.77	0.88 ± 0.81	2.69 ± 1.06
90	−0.14 ± 0.74	0.43 ± 2.55	2.79 ± 1.01

[a] The antenna temperature at each DMR frequency of Galactic emission traced by template map X is $T_A = \alpha X$ μK.
[b] α has units μK K^{-1}, since the template map has units K.
[c] α is dimensionless, since the template map has units μK.
[d] α has units μK (MJy sr^{-1})$^{-1}$, since the template map has units MJy sr^{-1}.

high-latitude pixel[9] (Hinshaw et al. 1996). In the limit that only instrument noise is considered, the covariance matrix $\boldsymbol{M}$ is diagonal and equation (2) reduces to a least-squares estimate of α. We do not work in this limit, but include the covariance between pixels or Fourier modes predicted for a scale-invariant spectrum of CMB anisotropy (for details see Górski et al. 1996 and Hinshaw et al. 1996). Equation (2) is easily generalized to fit multiple DMR frequencies and template maps simultaneously.

3. GALACTIC MICROWAVE EMISSION

Table 1 shows the fitted correlation coefficients between the 4 yr DMR maps and the Galactic templates, derived using equation (2) in a maximum likelihood analysis with the "brute-force" pixel basis (Hinshaw et al. 1996). We evaluate the three DMR frequencies simultaneously, $D = [T_{31}, T_{53}, T_{90}]$, and account for possible cross-talk between the synchrotron and far-IR templates by fitting both templates simultaneously, $G = [X^{\rm synch}, X^{\rm DIRBE}]$. The uncertainties in Table 1 include the errors from instrument noise, chance alignments between the CMB and Galactic features, and cross-talk between the two Galactic templates.

We find no statistically significant correlation between the DMR sky maps and either the 408 MHz survey or the cosmic-ray synchrotron model. Both synchrotron templates have deficiencies, and it is possible that neither template accurately reflects the distribution of synchrotron emission at millimeter wavelengths, regardless of overall normalization. The large-scale structure in the 408 MHz survey at $|b| > 20°$ is dominated by the North Polar Spur (Loop I), but this region has a steeper spectral index and becomes increasingly less important at higher frequencies (Lawson et al. 1987). The cosmic-ray model accounts for both the spatial variation in $\beta_{\rm synch}$ and the steepening of the spectrum at higher frequencies, but the spatial structure of this model at the DMR frequencies is dominated by regions of flattened index at the southern declination limits of the 1420 MHz survey (Reich & Reich 1988) used to generate this model. The DMR maps show no evidence for such bright regions, suggestive instead of sidelobe pickup at the southern declination limits of the 1420 MHz survey. Table 2 shows the rms fluctuations in antenna temperature corresponding to the fitted coefficients. We adopt an upper limit $\Delta T_{\rm synch} < 11$ μK (95% confidence) at 31.5 GHz for emission traced by either synchrotron template.

Tables 1 and 2 show a statistically significant correlation between the DMR maps and the DIRBE 140 μm map; we obtain nearly identical results using the DIRBE maps at 100 and at 240 μm. Note that the Galactic emission has nearly equal amplitude in the DMR 53 and 90 GHz channels but rises sharply at 31.5 GHz (Table 2). The frequency dependence of the inferred signal in the DMR maps is well described by a superposition of dust and free-free emission. We fit the rms DMR and DIRBE signals to emission models of the form $I_\nu = \tau(\nu/\nu_0)^\beta B_\nu(T) + A_{\rm ff}(\nu/\nu_0)^{-0.15}$, i.e., a model with a single dust population with enhanced submillimeter emissivity plus free-free emission. The best fit occurs for dust temperature $T = 20.0^{+2.5}_{-4.0}$ K and emissivity $\beta = 1.5^{+1.1}_{-0.3}$, with opacity $\tau = (1.2^{+0.7}_{-0.4}) \times 10^{-5}$ (68% confidence). The fitted amplitudes correspond to $\Delta T_{\rm dust} = 2.7 \pm 1.3$ μK and $\Delta T_{\rm ff} = 7.1 \pm 1.7$ μK for the rms fluctuations in dust and free-free antenna temperature at 53 GHz. The amplitude of this emission, however, is small compared to the rms CMB anisotropy, $\Delta T_{\rm CMB} = 29 \pm 1$ μK (Bennett et al. 1996).

TABLE 2

Root Mean Square Galactic Signal in DMR Sky Maps (μK)[a]

DMR Frequency (GHz)	Galactic Template		
	408 MHz	Cosmic Ray	DIRBE 140 μm
31.5	5.7 ± 5.5	8.4 ± 5.5	22.7 ± 5.4
53	3.4 ± 3.7	3.9 ± 3.6	9.6 ± 3.8
90	−0.7 ± 3.6	1.9 ± 3.5	10.0 ± 3.6

[a] Units are antenna temperature. The quadrupole has not been subtracted.

The correlation technique is insensitive to emission whose spatial distribution is uncorrelated with the Galactic template maps. We estimate the amplitude of the total free-free emission (including any uncorrelated component) by analyzing a linear combination of the DMR maps designed to be sensitive to free-free emission (spectral index −2.15 in units of antenna temperature), cancel emission with a CMB spectrum, and minimize instrument noise:

$$T_{\rm ff} = 0.37[\tfrac{1}{2}(T'_{31A} \pm T'_{31B})] + 0.02[\tfrac{1}{2}(T'_{53A} \pm T'_{53B})] - 0.47[\tfrac{1}{2}(T'_{90A} \pm T'_{90B})], \quad (3)$$

where T' is the antenna temperature in each DMR channel after subtracting synchrotron and dust emission using the cosmic-ray and DIRBE models, respectively. We smooth the maps with a 7° FWHM Gaussian to further reduce the effects of noise, remove a fitted monopole and dipole, and compare the variance of the (A + B)/2 sum map to the (A − B)/2 difference map. We obtain an estimate for the fluctuations in free-free antenna temperature at 53 GHz from all sources, $\Delta T_{\rm ff} = 5.2 \pm 4.2$ μK. This value compares well with the correlated component at the same effective smoothing, $\Delta T_{\rm ff} = 6.8 \pm 2.6$ μK. We further test for free-free emission uncorrelated with the far-IR dust by removing the correlated free-free component from each DMR channel prior to forming the free-free linear combination (eq. [3]). A power spectrum analysis of this uncorrelated free-free map shows no statistically significant signal at any $\ell < 30$. The correlated component must form at least a third of the total free-free emission (95% confidence) and may form the bulk of this emission.

4. QUADRUPOLE

The quadrupole represents one order of a spherical harmonic expansion of the temperature distribution in the sky

[9] For computational reasons the direct pixel basis uses maps degraded one step in pixel resolution, leaving 954 high-latitude pixels, each of diameter 5°.2.

TABLE 3

QUADRUPOLE COMPONENTS IN UNCORRECTED SKY MAPS[a]

Map	Q_1	Q_2	Q_3	Q_4	Q_5	$Q_{\rm rms}$[b]
DMR 31.5 GHz[c]	−29.1 ± 12.6	27.0 ± 6.5	2.1 ± 6.0	4.5 ± 12.8	5.3 ± 11.9	15.6 ± 5.4
DMR 53 GHz[c]	−13.6 ± 7.7	9.5 ± 2.7	3.8 ± 2.2	0.0 ± 8.2	3.5 ± 7.6	4.4 ± 3.3
DMR 90 GHz[c]	0.2 ± 8.5	5.0 ± 3.5	6.7 ± 2.8	−0.3 ± 9.1	3.2 ± 8.3	0.0 ± 3.0
408 MHz[d].....	−6.6	3.4	−0.1	5.5	−1.8	4.5
Cosmic ray[e].....	−5.2	2.7	−1.3	5.9	−1.3	4.2
DIRBE 140 μm[f].....	−6.6	1.7	−1.3	1.9	−1.4	3.4

[a] The Doppler quadrupole has been removed from the DMR maps.
[b] $Q_{\rm rms}$ has been corrected for statistical bias (see text).
[c] Map units are μK thermodynamic temperature.
[d] Map units are K antenna temperature.
[e] Map units are μK antenna temperature.
[f] Map units are MJy sr^{-1}.

maps. After the low-latitude portion of the sky map is excised, the spherical harmonic functions $Y_{\ell m}(l, b)$ are no longer orthogonal on the remaining sky pixels, allowing power from higher orders to be aliased into the quadrupole (and vice versa). Górski et al. (1996) address this problem by constructing a new set of basis functions orthogonal on the cut sky. In what follows, we retain the more familiar spherical harmonic basis and minimize aliasing by including a theoretical model for the higher orders ($\ell \geq 3$) of the power spectrum. We derive the quadrupole parameters Q_i by minimizing

$$\chi^2 = \sum_{a,b} \left[T^{\rm DMR} - \left(\sum_{i=1}^{5} Q_i B_i \right) \right]_a (\boldsymbol{M}^{-1})_{ab} \left[T^{\rm DMR} - \left(\sum_{i=1}^{5} Q_i B_i \right) \right]_b , \quad (4)$$

in a pixel-based maximum likelihood analysis, where B_i are the quadrupole basis functions (Bennett et al. 1992) and the 954×954 covariance matrix $\boldsymbol{M}$ is defined for a scale-invariant CMB model (cf. eq. [1] of Hinshaw et al. 1996). That is, we describe the high-latitude sky as a fixed quadrupole pattern plus a statistical distribution of higher order power given by a Harrison-Zeldovich power spectrum. Table 3 shows the quadrupole parameters Q_i fitted to the high-latitude portion of the (A + B)/2 sky maps, without Galactic correction. The quadrupole parameters for the Galactic template maps are also shown.

The Galaxy is a strong quadrupolar source. We derive the CMB quadrupole parameters as follows. We correct each DMR map for the second-order Doppler quadrupole $[Q_1, Q_2, Q_3, Q_4, Q_5] = [0.9, -0.2, -2.0, -0.9, 0.2]$ μK thermodynamic temperature caused by the motion of the solar system with respect to the CMB rest frame. We remove Galactic emission using the synchrotron and DIRBE templates by adding terms to equation (4) of the form $\alpha_{\rm synch} X^{\rm synch} \nu^{\beta_{\rm synch}} + \alpha_{\rm dust} X^{\rm DIRBE} \nu^{\beta_{\rm dust}} + \alpha_{\rm ff} X^{\rm DIRBE} \nu^{\beta_{\rm ff}}$ and fitting the three DMR frequencies simultaneously. Rather than fitting the synchrotron and DIRBE templates to each map independently, we use the results of § 3 and fit the templates to all three frequencies simultaneously, specifying the spectral behavior via the spectral indices. The free parameters in the fit are thus the synchrotron, dust, and free-free amplitude coefficients plus five CMB quadrupole parameters. Using the nominal values $\beta_{\rm synch} = -3$, $\beta_{\rm dust} = +2$, and $\beta_{\rm ff} = -2.15$, we derive correlation coefficients $\alpha_{\rm synch} = 0.27 \pm 0.20$ μK K^{-1}, $\alpha_{\rm dust} = 0.70 \pm 0.27$ μK

TABLE 4

CMB QUADRUPOLE PARAMETERS (μK)[a]

Q_1 (1)	Q_2 (2)	Q_3 (3)	Q_4 (4)	Q_5 (5)	$Q_{\rm rms}$[b] (6)
Cross-Correlation					
27.9 ± 4.7	0.6 ± 1.7	10.8 ± 1.6	−14.9 ± 4.9	19.0 ± 4.6	18.0 ± 2.3
19.0 ± 7.4	2.1 ± 2.5	8.9 ± 2.0	−10.4 ± 8.0	11.7 ± 7.3	10.7 ± 3.6
31.2 ± 12.5	1.0 ± 3.7	12.8 ± 3.7	−9.3 ± 13.4	−0.6 ± 12.1	11.7 ± 5.8
Linear Combination					
24.3 ± 6.2	−2.1 ± 3.1	8.3 ± 2.9	−18.9 ± 6.2	6.8 ± 6.0	14.6 ± 3.1
20.0 ± 9.1	−2.6 ± 3.9	9.4 ± 3.3	−6.1 ± 9.6	3.5 ± 8.8	7.1 ± 4.2
35.1 ± 14.3	−3.2 ± 4.9	12.7 ± 4.8	−7.1 ± 15.4	6.6 ± 13.8	12.2 ± 6.8
Systematic and Model Uncertainties					
8.2	2.7	2.5	4.3	10.4	7.1

[a] The three rows for each technique refer to Galactic cut $|b| > 15°$, $|b| > 20°$ with custom cutouts, and $|b| > 30°$. The Doppler quadrupole has been removed from the maps. Results are in thermodynamic temperature.
[b] $Q_{\rm rms}$ has been corrected for statistical bias (see text).

MJy^{-1} sr, and $\alpha_{\rm ff} = 2.07 \pm 0.49$ μK MJy^{-1} sr antenna temperature at 53 GHz. Table 4 shows the quadrupole parameters for the corrected CMB map. The uncertainties are dominated by aliasing of higher order power and to a lesser extent by instrument noise and chance alignments in the template map correlation.

The statistical uncertainties in Table 4 do not include the systematic effects associated with the choice of template map and spectral index. We evaluate the uncertainties associated with the Galactic spectral indices by repeating the analysis as $\beta_{\rm synch}$ is varied over the range $[-2.8, -3.3]$ and $\beta_{\rm dust}$ over the range [1.1, 2.0]. The differences are small, typically 10% of the statistical uncertainty. We estimate the uncertainties associated with the Galactic model techniques by repeating the CMB quadrupole analysis for several different Galactic models. The simplest change is to substitute the cosmic-ray synchrotron template for the 408 MHz survey. Synchrotron emission is faint at millimeter wavelengths, and both templates have similar quadrupoles: the estimated CMB quadrupole does not depend sensitively on the choice of synchrotron template or spectral index. Similarly, we may estimate the dust emission by fitting the DIRBE dust emission or scaling the FIRAS dust model (Wright et al. 1991). Differences between these techniques are small and are dominated by differences in the FIRAS and DMR beam shape. We estimate the systematic uncertainty in the free-free correction by comparing the quadrupole results using the DMR/DIRBE cross-correlation to the results using the linear combination technique. The results are in agreement with the less noisy cross-correlation technique (Table 4). Systematic effects associated with changing the Galactic model are typically 1–5 μK, smaller than the statistical uncertainties.

The largest systematic effect is the choice of Galactic cut angle. Table 4 shows the quadrupole parameters fitted for the regions $|b| > 15°$, $|b| > 20°$ with custom cutouts, and $|b| > 30°$. The changes in the fitted parameters as the Galactic cut is varied are comparable to the statistical uncertainties, and limit our ability to estimate the CMB quadrupole. Since statistically significant CMB features exist in the region $15° < b < 30°$, the change in fitted quadrupole parameters as the Galactic cut is varied reflects aliasing of higher order power as well as potential shortcomings in the Galactic models. We estimate the uncertainty from this effect as half of the spread in each quadrupole component. The bottom row of Table 4 shows the combined systematic uncertainty in each component, given by the quadrature sum of the separate uncertainties in spectral index, model techniques, Galactic cut, and the instrument systematic artifacts (Kogut et al. 1996b).

The quadrupole amplitude, $Q_{\rm rms}$, provides a convenient description of the CMB quadrupole. Since it is quadratic in the map temperatures, both instrument noise and aliasing will bias $Q_{\rm rms}$ toward higher values. The individual parameters Q_i are unbiased estimators, but they provide a less concise characterization. We correct for the bias by the quadrature subtraction of the rms statistical uncertainty: $Q^2_{\rm rms} = \frac{4}{15}(\sum_i \eta_i Q_i^2 - \sum \eta_i \delta Q_i^2)$, where the Q_i are the central values of the fitted quadrupole components, the δQ_i are the statistical uncertainties, and the η_i are the weights $[\frac{3}{4}, 1, 1, 1, 1]$ (Gould 1993). Column (6) of Table 4 (labeled $Q_{\rm rms}$) shows this debiased estimate for the CMB rms quadrupole amplitude.

Figure 2 (Plate L5) shows the CMB maps from the cross-correlation and linear combination techniques. Since the cross-correlation technique has the smallest random errors, we adopt the CMB quadrupole parameters from this model using the custom Galactic cut as a compromise between sky coverage and Galactic foreground emission. The resulting estimate of the CMB quadrupole amplitude is $Q_{\rm rms} = 10.7 \pm 3.6 \pm 7.1$ μK, where errors represent the statistical and systematic uncertainties, respectively. Allowing for the systematic uncertainty in the Galactic correction (which does not have a Gaussian distribution), the CMB quadrupole amplitude lies in the range [4, 28] μK at 95% confidence.

5. CONCLUSIONS

Cross-correlation of the DMR maps with either the 408 MHz synchrotron survey or a cosmic-ray synchrotron model with spatially varying spectral index yields upper limits to fluctuations in synchrotron emission traced by either template, $\Delta T_{\rm synch} < 11$ μK at 31.5 GHz. If either template correctly reproduces the angular distribution of synchrotron emission, the amplitude normalization requires a mean spectral index between 408 MHz and 31.5 GHz of $\beta_{\rm synch} < -3.0$.

Cross-correlation of the DMR maps with the dust-dominated DIRBE 140 μm survey shows a statistically significant signal whose dependence on DMR frequency is consistent with a superposition of dust and free-free emission. The rms amplitude of the dust signal is $\Delta T_{\rm dust} = 2.7 \pm 1.3$ μK antenna temperature at 53 GHz, including the contribution from the quadrupolar component. The dust emission may be used to place a lower limit on enhanced emissivity from 140 μm to 6 mm wavelength: $\beta_{\rm dust} > 1.1$ at 95% confidence.

We detect a component of the free-free emission from the warm ionized interstellar medium that is correlated with the far-infrared dust on angular scales of 7° or larger. The amplitude of the correlated free-free emission, $\Delta T_{\rm ff} = 7.1 \pm 1.7$ μK, compares well with the total free-free emission from all sources, derived from a linear combination of the DMR maps. The correlated component must form at least a third of the total free-free emission (95% confidence) and may form the bulk of this emission.

Galactic emission is comparable to the CMB on quadrupolar scales and is counteraligned to the CMB in several of the five components. *The fitted quadrupole in the uncorrected DMR maps is not representative of the CMB quadrupole in either amplitude or phase*. Analysis of the DMR maps that includes the quadrupole anisotropy should correct for Galactic emission, using either the cross-correlation technique or the noisier linear combination technique. We correct the DMR channel maps for Galactic emission using both techniques and estimate the quadrupole components using a maximum likelihood analysis. The random statistical uncertainties are dominated by the aliasing of power from higher multipole orders. After correction for the positive bias from noise and aliasing, the CMB quadrupole amplitude observed at high latitude is $Q_{\rm rms} = 10.7 \pm 3.6 \pm 7.1$ μK, where the uncertainties represent the random statistical errors and systematic modeling errors, respectively.

We are grateful to Charley Lineweaver for helpful discussion. We acknowledge the dedicated efforts of the many people responsible for the *COBE* DMR data: the NASA Office of Space Sciences, the *COBE* flight team, and all of those who helped process and analyze the data.

PLATE L5

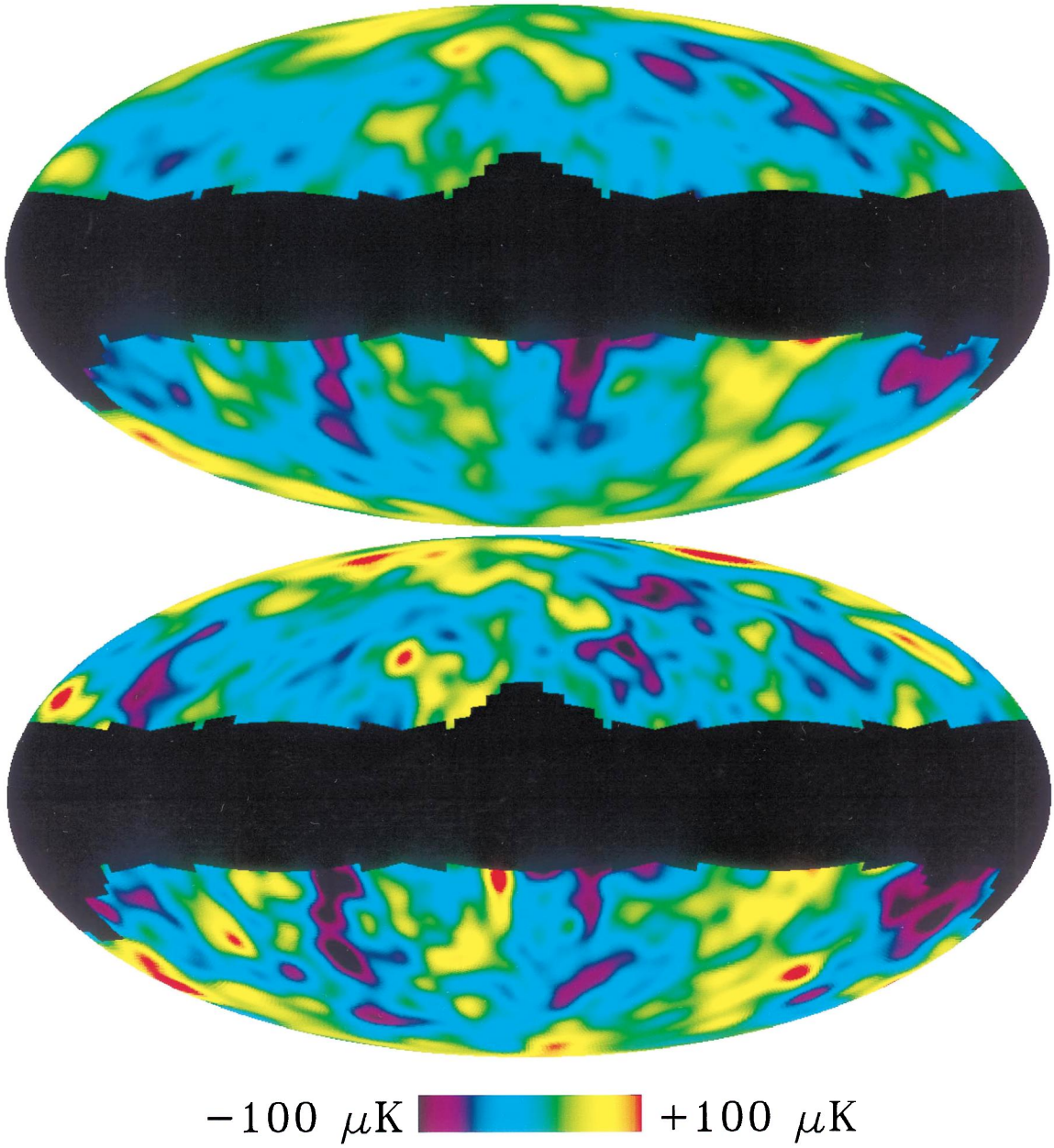

FIG. 2.—Maps of the cosmic microwave background anisotropy after removing Galactic emission; Mollweide projection in Galactic coordinates. *Top*: Cross-correlation technique. *Bottom*: Linear combination technique. The Galactic models do not attempt to fit the Galactic plane; only the high-latitude portion is shown. The cross-correlation technique represents a compromise between removing faint Galactic emission and minimizing instrument noise.

KOGUT et al. (see 464, L8)

REFERENCES

Banday, A., & Wolfendale, A. W. 1991, MNRAS, 248, 705
Bennett, C. L., et al. 1992, ApJ, 396, L7
———. 1996, ApJL, 464, L1
Davies, R. D., Watson, R. A., & Gutiérrez, C. M. 1996, MNRAS, 278, 925
Désert, F.-X., Boulanger, F., & Puget, J.-L. 1990, A&A, 327, 215
Górski, K. M., Banday, A. J., Bennett, C. L., Hinshaw, G., Kogut, A., Smoot, G. F., & Wright, E. L. 1996, ApJL, 464, L11
Gould, A. 1993, ApJ, 403, L51
Haslam, C. G. T., Klein, U., Salter, C. J., Stoffel, H., Wilson, W. E., Cleary, M. N., Cooke, D. J., & Thomasson, P. 1981, A&A, 100, 209
Hinshaw, G., Banday, A. J., Bennett, C. L., Górski, K. M., Kogut, A., Smoot, G. F., & Wright, E. L. 1996, ApJL, 464, L17
Kogut, A., Banday, A. J., Bennett, C. L., Górski, K. M., Hinshaw, G., & Reach, W. T. 1996a, ApJ, 460, 1
Kogut, A., Banday, A. J., Bennett, C. L., Górski, K. M., Hinshaw, G., Smoot, G. F., & Wright, E. L. 1996b, ApJL, 464, L29
Lawson, K. D., Mayer, C. J., Osborne, J. L., & Parkinson, M. L. 1987, MNRAS, 225, 307
Reach, W. T., Franz, B. A., Kelsall, T., & Weiland, J. L. 1995, in Unveiling the Cosmic Infrared Background, ed. E. Dwek (New York: AIP), 37
Reich, P., & Reich, W. 1988, A&AS, 74, 7
Wright, E. L., et al. 1991, ApJ, 381, 200